minerals

MDPI

Article

Manganese-Containing Inclusions in Late-Antique Glass Mosaic Tesserae: A New Technological Marker?

Alberta Silvestri [1,*], Fabrizio Nestola [1] and Luca Peruzzo [2]

[1] Dipartimento di Geoscienze, Università degli studi di Padova, via G. Gradenigo 6, 35131 Padova, Italy; fabrizio.nestola@unipd.it

[2] Consiglio Nazionale delle Ricerche (CNR), Istituto di Geoscienze e Georisorse (IGG), sede di Padova, via G. Gradenigo 6, 35131 Padova, Italy; luca.peruzzo@igg.cnr.it

* Correspondence: alberta.silvestri@unipd.it; Tel.: +39-049-8279142

Received: 10 September 2020; Accepted: 2 October 2020; Published: 3 October 2020

Abstract: The present study focuses on manganese-containing inclusions identified in late-Antique glass tesserae, light brown/amber and purple in colour, from Padova (Italy), in order to clarify the nature of these inclusions, never identified in glass mosaics until now, and provide new insights on the production technologies of such kinds of tesserae. Multi-methodological investigations on manganese-containing inclusions were carried out in this work by means of optical microscopy (OM), scanning electron microscopy (SEM), micro-X-ray diffraction (micro-XRD), electron backscattered diffraction (EBSD), electron microprobe (EMPA), and micro-Raman spectroscopy. The combination of analytical results shows that inclusions are crystalline, new-formed phases, mainly composed of manganese, silica and calcium, and are mineralogically ascribed as a member of the braunite-neltnerite series, with unit-cell parameters closer to those of neltnerite. However, the low Ca content makes such crystalline compounds more similar to braunite, in more detail, they could be described as Ca-rich braunite. The occurrence of such crystalline phase allows us to constrain melting temperatures between 1000 and 1150 °C, and to hypothesize pyrolusite, MnO_2, as the source of manganese. In addition, it is worth underlining that the same phase is identified in tesserae characterised by different colours (light brown/amber vs purple due to different manganese/iron ratios), glassy matrices (soda-lime-lead vs soda-lime) and opacifiers (cassiterite vs no opacifier). This suggests that its occurrence is not influenced by the "chemical environment", revealing these manganese-containing inclusions as a new potential technological marker.

Keywords: late-Antique glass tesserae; manganese; crystalline inclusions; OM; SEM-EDS-EBSD; micro-XRD; EMPA; micro-Raman spectroscopy; braunite-neltnerite; melting temperature

1. Introduction

In ancient glass production, manganese acts both as colourant and decolourant (e.g, [1]). In the former case, when Mn^{3+} is generally in excess of 1%, it imparts a pink/purple colour (e.g., [2–4]), and its use as a colourant is attested throughout the whole history of glass production, from the Bronze Age until the Modern Epoch (e.g., [5]). Manganese acts as a decolourant, taking part in the redox equilibria with iron, in accord to the well-known reaction: $Fe^{2+} + Mn^{3+} \leftrightarrow Fe^{3+} + Mn^{2+}$ (e.g., [6]). The Mn^{2+} ion is not chromophorous, but the purple colour of Mn^{3+} counterbalances the yellow of Fe^{3+}, producing a decolourant effect on glass. Thus, manganese can be considered as having both a physical and a chemical action on the iron colouring [1]. The use of manganese as a decolourant increased from the 4th century AD until Medieval times, when it became the only one used (e.g., [7–9]). However, the colouring/decolouring effects of manganese in glass are rather complex, being influenced by many parameters (compositions of batch, raw materials used as source of manganese, presence of

additives as sulphates or carbon, melting conditions). Also, Bidegaray et al. [10,11] recently tried to understand both why manganese-containing glass could be purple or colourless, in spite of having very similar chemical compositions, and how thickness, iron redox and antimony/manganese influence "perceived" and "intrinsic" colour in glass. In the past, manganese was likely introduced by treating Mn-bearing minerals (see Supplementary Table 1 in [9] for a list of primary and secondary Mn-common minerals). Pyrolusite (MnO_2) is one of the most common manganese minerals and, probably, the major manganese source in the past, although pyrolusite often occurs in association with other, less common, Mn-phases, such as in the wad, the mining name given to manganese ores mainly composed of manganese oxides/hydroxides, often of poor crystallinity. This may imply a more broadly diversified supply of manganese-bearing minerals, with respect to the exclusive use of pure pyrolusite [9,12,13].

In any case, regardless of the possible causes of different colours in manganese-containing glass and the various sources of manganese, it is commonly accepted that this element lies in glassy matrix as cation, forming redox couple with iron (e.g, [14,15]), but the presence of crystalline manganese-bearing compounds in ancient glass vessels and mosaics has never been documented, until now.

The present study focuses on manganese-containing inclusions identified into some late-Antique glass tesserae, light brown/amber or purple in colour, from Padova (Italy), with the aim of clarifying the nature of these inclusions and providing new insights on the production technologies of such kind of tesserae.

2. Materials and Methods

Glass tesserae comes from one of the only two palaeo-Christian mosaics known in the Veneto region (Italy), i.e., the one which originally decorated the votive chapel of St. Prosdocimus located in the basilica of St. Justine in Padova. These tesserae are 6th century AD in age and are characterised by a full range of colours (blue, yellow, orange, red, brown, green, white, and "gold") [16–18]. Manganese-containing inclusions are detected in all the tesserae of chromatic groups "light brown/amber" (NC) and "purple" (PR) for a total number of 10 tesserae (Figure 1). These tesserae were characterised from the archaeometric viewpoint with particular attention to identification of glassy matrices, opacifiers and colourants, and detailed results are reported in Silvestri et al. [18] and summarised in Table 1.

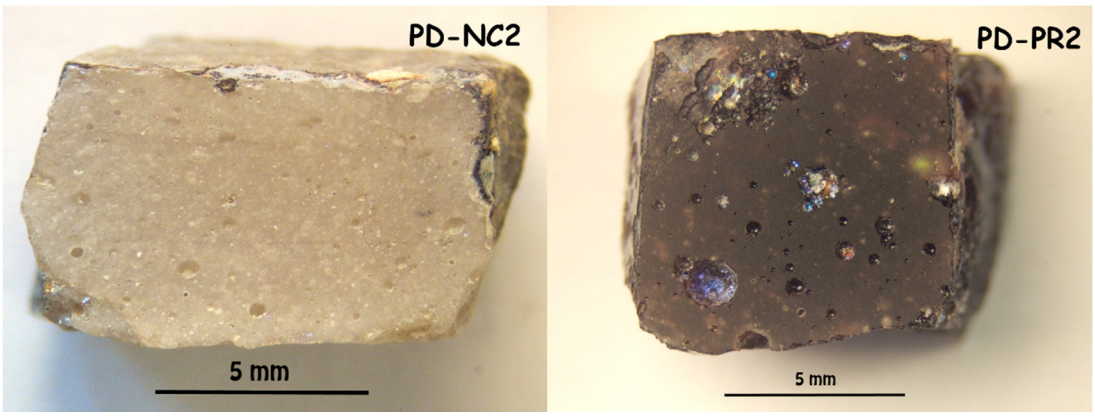

Figure 1. Pictures of two glass tesserae from Padova, representative of the two chromatic groups with manganese-containing inclusions: "Light brown/amber" (PD-NC2) and "purple" (PD-PR2).

The following multi-methodological approach was used here for the characterisation of manganese-containing inclusions: optical microscopy (OM) and scanning electron microscopy coupled with energy-dispersive X-ray spectrometry (SEM-EDS) for high-resolution morphologic inspection of inclusions and qualitative chemical analyses; electron microprobe (EMPA) to determine quantitative chemical composition of inclusions; micro-X-Ray (micro-XRD) and electron back-scattered diffraction (EBSD), and micro-Raman spectroscopy to definitively identify the crystalline phase.

Table 1. Summary of the main archaeometric results obtained on light brown/amber and purple tesserae from palaeo-Christian mosaic of St. Prosdocimus (Padova, Italy), showing the manganese-containing inclusions, which are the object of the present paper. In the case of chemical composition of tesserae, note that total iron and total manganese are expressed as FeO and MnO, respectively; in addition, contents of cobalt, copper, zinc, and antimony were also measured, but not reported here, because these elements are all under EMPA detection limits, equal to 0.03 wt% for CoO and CuO, and 0.04 wt% for ZnO and Sb_2O_3 (raw data from [18]).

Chromatic Group	Number of Samples	Label	Mean Chemical Composition, Expressed as Weight Percentage of the Element Oxides (in Bold), and Standard Deviations (in Italic) (EMPA Data)													
			SiO_2	**Na_2O**	**CaO**	**Al_2O_3**	**K_2O**	**MgO**	**FeO**	**TiO_2**	**MnO**	**P_2O_5**	**SO_3**	**Cl**	**SnO_2**	**PbO**
Light brown/amber	5	PD-NC from 1 to 5	**66.8**	**18.1**	**7.0**	**2.00**	**0.50**	**0.98**	**0.90**	**0.13**	**1.31**	**0.11**	**0.34**	**1.12**	**0.26**	**0.90**
			0.7	*0.1*	*0.2*	*0.02*	*0.03*	*0.06*	*0.06*	*0.01*	*0.11*	*0.06*	*0.03*	*0.06*	*0.03*	*0.11*
Purple	5	PD-PR from 1 to 5	**65.78**	**17.04**	**8.36**	**2.34**	**0.65**	**1.09**	**0.93**	**0.15**	**2.18**	**0.09**	**0.37**	**0.93**	**<0.04**	**<0.08**
			0.65	*0.17*	*0.14*	*0.03*	*0.09*	*0.11*	*0.07*	*0.02*	*0.20*	*0.04*	*0.06*	*0.22*		

Chromatic Group	Glassy Matrix	Reference Group	Opacifier	Colourant/Decolourant	MnO/FeO (Mean in Bold; st. dev. in Italic)
Light brown/amber	Soda-lime-lead	Série 3.2 of Foy et al. 2003 [44]	Cassiterite	Iron and manganese	**1.5**
					0.1
Purple	Soda-lime	Group 2 of Foy et al. 2003 [44]	None	Iron and manganese	**2.37**
					0.40

Optical microscopy observations were conducted under stereoscopic vision with a Zeiss Stemi 2000C microscope and under reflected light with a Nikon Eclipse Me600, both located in the Department of Geosciences (University of Padova, Padova, Italy). In the case of reflected light microscope, observations were carried out both using bright-field (BF) and dark-field (DF) illumination.

SEM analysis was performed on a FEI Quanta 200 FEG-ESEM instrument (CNR-ICMATE, Padova, Italy), coupled with an EDAX Genesis energy-dispersive X-ray spectrometer (EDS). SEM images were taken by collecting the backscattered electron signal (BSE), operating in medium-vacuum condition (<4 Pa), with an accelerating voltage of 25 kV and a working distance of about 10 mm. The high voltage conditions assure a good image contrast and the possibility of carrying out the EDS chemical analyses without changing microscope conditions.

The electron microprobe used for quantitative chemical analyses of inclusions was a CAMECA-SX50 (CNR-IGG, Padova, Italy), equipped with four wavelength-dispersive spectrometers (WDS). The detailed EMPA analytical conditions (measured elements and lines, used analyser crystals, current and voltage of electron beam, measure acquisition time, selected standards and detection limits) are given in Table 2. X-ray counts were converted to oxide weight percentages using the PAP (CAMECA) correction program. Precision and accuracy were within 1% for major elements and about 3–4% for minor elements and were checked against the $MnTiO_3$ standard. With EMPA, chemical compositions of inclusions were carried out by random point microanalyses (generally 20 per sample) and mean and standard deviations were calculated. In order to minimize the potential contamination by the glassy matrix around the manganese-containing inclusions, characterised by little dimensions (as detailed in the section on "Results and Discussion"), the EMPA spot size was reduced to about 1 μm in diameter, and analytical points were performed on the biggest crystals and, preferentially, in the center, avoiding the borders. In addition, in order to check the "quality" of each analytical point performed on inclusions, and to verify the absence of contamination by the surrounding glassy matrix, sodium was used as "control element"; only analyses, with Na contents comparable to the analytical point showing the lowest content of that element for each crystal, were chosen, since they were considered representative of the only manganese-inclusions, without the contribution of the glassy matrix.

Table 2. EMPA analytical conditions for manganese-containing inclusions. Analyser crystals used: LiF (lithium fluoride with d_{200} = 2.01 Å), PET (pentaerythritol with d_{002} = 4.37 Å) and TAP (thallium acid phthalate with d_{100} = 12.84 Å).

Element	Line	Analyser Crystal	Electron Beam		Acquisition Time (s)		Standard	Detection Limits (wt%)
			nA	kV	Peak	Background		
Na	K_a	TAP 100	2	20	10	5	Albite	0.02
Mg	K_a	TAP 100	2	20	10	5	Diopside	0.01
Al	K_a	TAP 100	2	20	10	5	Al_2O_3	0.08
Si	K_a	TAP 100	2	20	10	5	Diopside	0.08
Ca	K_a	PET 002	2	20	10	5	Diopside	0.08
Ti	K_a	PET 002	2	20	10	5	$MnTiO_3$	0.08
Mn	K_a	LiF 200	2	20	10	5	$MnTiO_3$	0.02
Fe	K_a	LiF 200	2	20	10	5	Fe_2O_3	0.03

Micro-X-ray diffraction patterns were carried out by using a Supernova Rigaku-Oxford Diffraction diffractometer (Oxford Diffraction) equipped with an X-ray micro-source assembled with a Pilatus 200 K Dectris detector (Department of Geosciences, University of Padova, Padova, Italy). The micro-X-ray source, MoKα (0.7107 Å), operates at 50 kV and 0.8 mA, with a spot size of 0.12 mm. The sample-to-detector distance was 68 mm. In the present analysis, data were collected

in micro-X-ray powder diffraction mode, simulating a Gandolfi camera measurement mode, due to the polycrystalline nature of the samples. Micro-XRD analytical data were processed by the X'Pert HighScore (PANalytical copyright); 2θ Bragg angles and *d* spacing values were calculated with the second-derivative algorithm of Savitzky and Golay [19].

The EBSD analyses were performed on a FEI Quanta 450 FEG-ESEM (Centre of Excellence Telč, Telč, Czech Republic), operating in high-vacuum condition (10^{-4} Pa), with an accelerating voltage of 25 kV and a working distance of 16 mm.

Micro-Raman spectra were collected between 100 and 3500 cm^{-1} using a DXR Thermo Scientific Raman spectrometer (Department of Chemical Sciences, University of Padova, Padova, Italy), equipped with 532 nm laser source. Spectra were collected using a 50x LWD (Long Working Distance) objective and a power of 5 mW. The estimated spectral resolution was between 2.7 and 4.2 cm^{-1} and the spatial resolution was estimated to be about 1.1 μm. The acquisition time adopted was 10 s for 40 scans stereoscopic accumulation. Phase identification was carried out by comparisons among the acquired spectra and those reported in the RRUFF™ database project website (https://rruff.info/, [20]).

Except for stereoscopic optical microscopy conducted on the whole tesserae, all other analyses were performed on polished sections obtained by cutting layers, about 500 μm in thickness, with a diamond-coated saw from the back of each tessera. These layers were mounted in epoxy resin and thin-sectioned to 50 μm thick; the surfaces of each section were then polished with a series of diamond pastes down to 1 μm grade and coated with a conductive carbon film for EMPA and SEM-EDS analyses; for EBSD analysis, sections were further polished by means of a vibratory polisher with colloidal silica and finally coated with a very thin layer of carbon. Polished sections without carbon coating film were employed for OM observations, micro-XRD analysis and micro-Raman spectroscopy.

3. Results and Discussion

Micro-textural characterisation of manganese-containing inclusions dispersed in the glassy matrix was carried out by OM and SEM-BSE analyses. In "light brown/amber" (NC) and "purple" (PR) tesserae, the inclusions are sporadic and small in size (<100 μm). In OM images under reflected light, they appear greyish white with a medium reflectance in BF illumination and dark brown in colour in DF illumination (Figure 2).

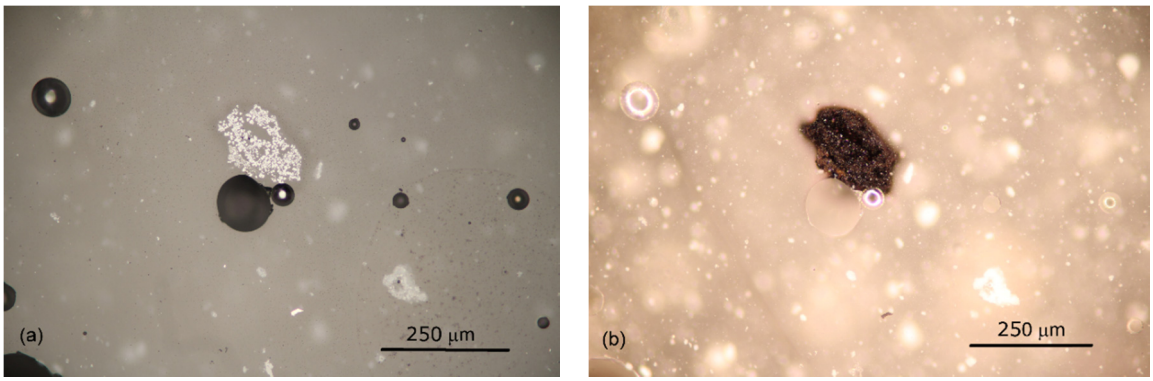

Figure 2. OM images of manganese-containing inclusions of tessera PD-NC2. Note that they appear greyish white with a medium reflectance in BF illumination (**a**) and dark brown in colour in DF illumination (**b**). This is the same for all the tesserae with these kinds of inclusions.

SEM-BSE images show that the inclusions, which are brighter than glassy matrix, are composed of aggregates of micro-crystals, euhedral in habit and with diameters generally <10 μm each (Figure 3). The polygonal forms, shown by the micro-crystals, suggest that they are new-formed phases, precipitated into the glassy matrix. In all tesserae, the EDS data show that all the inclusions basically have the same composition and are composed of manganese, silicon and calcium (Figure 3). This may

indicate that micro-crystals belong to the same phase in all samples investigated regardless of the macroscopic colour of tessera.

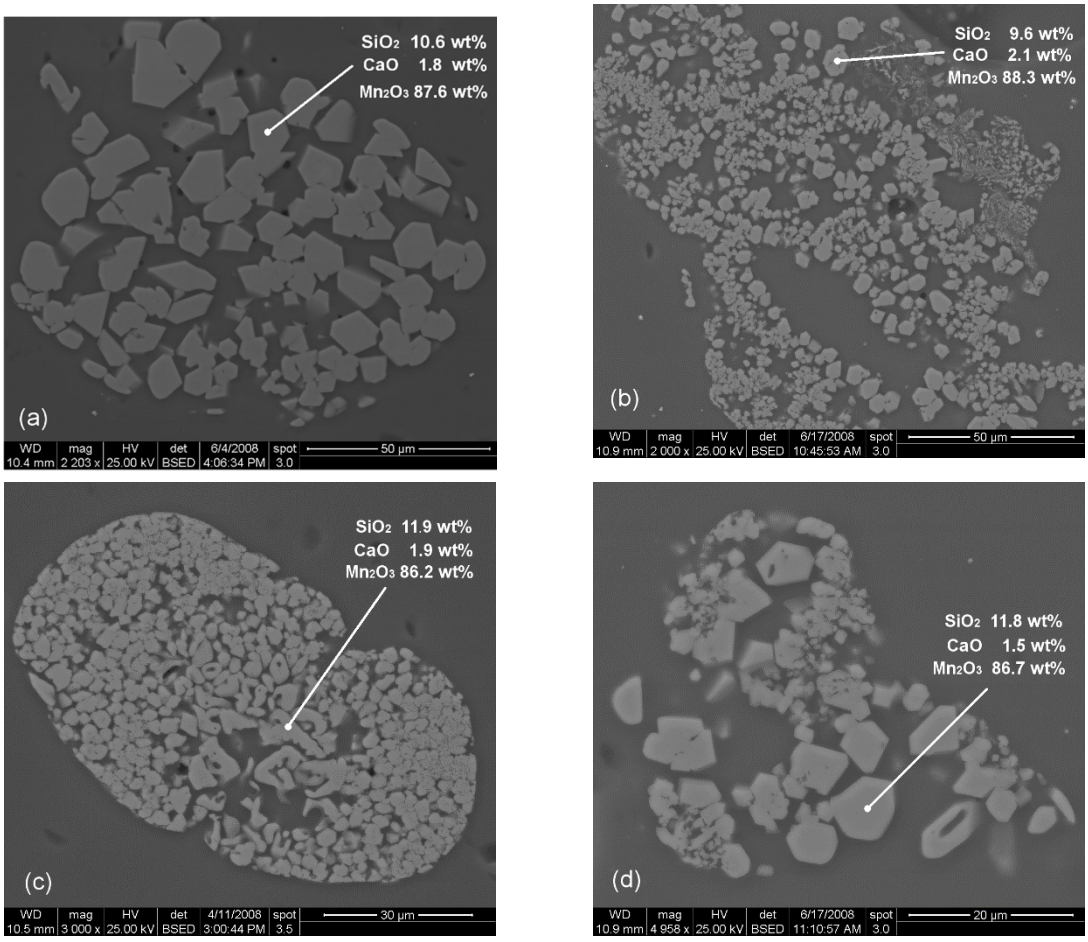

Figure 3. SEM-BSE images of manganese-containing inclusions in Padova tesserae PD-NC1 (**a**), PD-NC2 (**b**), PD-PR2 (**c**) and PD-PR3 (**d**). Note the same micro-texture and habit of manganese aggregates, independently from chromatic group. EDS compositional data are also reported within each image.

In order to perform an in-deep investigation of the nature of such inclusions, micro-mineralogical analyses were performed by means of micro-XRD and EBSD analyses, micro-Raman spectroscopy, and quantitative chemical analyses by means of EMPA.

Both micro-XRD and EBSD analyses confirmed that the manganese-rich phase is certainly crystalline.

The micro-XRD pattern obtained directly from the polished thin section (Figure 4a), shows that the manganese-containing inclusions can be ascribed to a member of the braunite-neltnerite series.

Braunite ($Mn^{2+}Mn^{3+}{}_6SiO_{12}$) is one of the more common manganese ore minerals, and together with bixbyite $(Mn,Fe)_2O_3$, braunite II ($Ca_{0.5}Mn^{3+}{}_7Si_{0.5}O_{12}$) and neltnerite ($CaMn^{3+}{}_6SiO_{12}$) is a member of a polysomatic series containing Mn^{3+}, whose structural and chemical features were previously described in Geller [21], de Villiers and Herbstein [22], de Villiers [23,24], Baudracco-Gritti et al. [25], Baudracco-Gritti [26], de Villiers and Buseck [27] and de Villiers et al. [28]. The composition of these minerals can be described by the general formula M_8O_{12}, through substitutions of Si^{4+}, Mn^{2+} and Ca^{2+} for Mn^{3+}, by having, as a consequence, a considerable range of compositions. The structural relations among these minerals are also complex. While bixbyte, which contains >0.75 mol% Fe, is cubic with space group Ia3, pure Mn_2O_3, named partridgeite is rhombic, pseudo-cubic [21]. Braunite, braunite II and neltnerite are isostructural; they have the same tetragonal space group $I4_1/acd$, and their

structural arrangement is composed of one distorted cubic [$Mn^{2+}O_8$] site, three non-equivalent distorted [$Mn^{3+}O_6$] octahedra, and one [$Si^{4+}O_4$] tetrahedron [23,27]. In natural braunites, the sites occupied by Mn^{3+} can contain minor quantities of Fe^{3+} and Al, whereas Mn^{2+} can be replaced by Ca and small amounts of Mg, Cu, Ti, Ba, Na and K [26,29–31]. Various arrangements of layers (modules) parallel to (001), stacked in various proportions and with different stacking vectors, influence c-axis dimension in the above three members, which have the following cell parameters: (a: 9.42, 9.46, 9.43 Å and c: 18.70, 18.85, 37.77 Å in braunite [23], neltnerite [25], and braunite II [24], respectively).

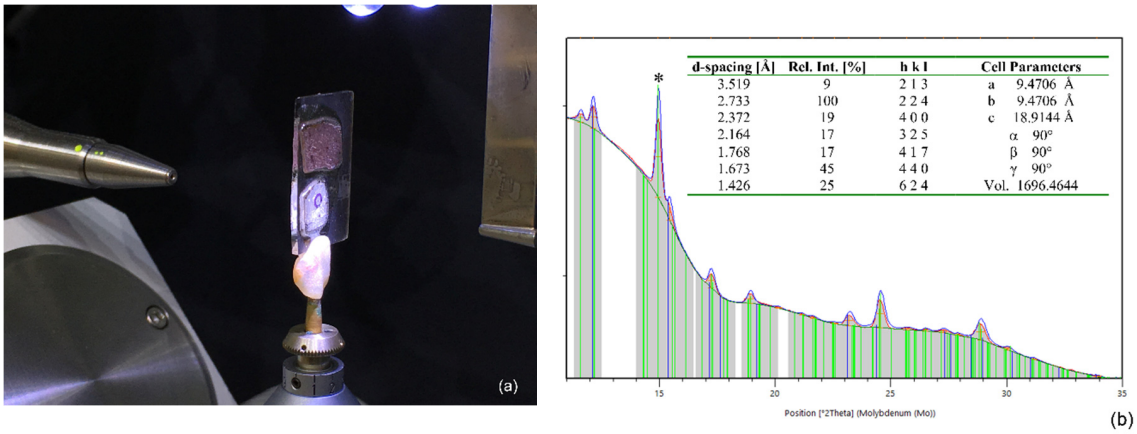

Figure 4. (**a**) Instrumental configuration of micro-XRD measurements, carried out directly on a polished thin-section, where two tesserae (one purple on the top—PD-PR1, and one light brown/amber on the bottom—PD-NC1) were mounted; note that the sample analysed is located within the black circle visible on the light brown/amber tessera; (**b**) micro-XRD pattern of tessera PD-NC1. In the table inset, list of peaks (showing *d*-spacing, relative intensity and *hkl* indices) and cell parameters of manganese-containing inclusion. Note that the peak identified by *, having d_{hkl} equal to 3.36 Å, is assigned to cassiterite (the main opacifier of NC tesserae from Padova, and it is not considered in the present paper).

According to chemical analyses reported into Baudracco-Gritti [26], an almost continuous solid solution between braunite and braunite II was found, following the general formula [32]:

$$(Mn^{2+}{}_{1-2x}\ Ca_x)^{VIII}\ Mn^{3+}{}_{6+2nx}{}^{VI}\ Si_{1-x}{}^{IV}\ O_{12}\ (\text{with } x \leq 0.5;\ n \leq 1) \quad (1)$$

On the contrary, in the samples analysed by Baudracco-Gritti [26], it seems that there is no demonstrable continuous solid solution series between braunite and neltnerite, although evidence of Ca substitution in braunites is documented. De Villiers at al. [28] explain the observed discontinuity probably due to insufficient chemical data, because there is not any obvious crystal chemical explanation, as also demonstrated experimentally by Anastasiou and Langer [33], who noted Mn^{2+}/Ca exchange in braunite up to $(Ca_{0.8}Mn^{2+}{}_{0.2})Mn^{3+}{}_6SiO_{12}$ at P = 15 kb, T = 800 °C, and fO_2 of the Mn_2O_3/MnO_2 buffer. Indeed, it would seem quite feasible to have a continuous variation in the Ca/Mn^{2+} ratio on the cubic distorted site, and the extent of distortion should not create a barrier for the continuous exchange of Mn^{2+} or Ca atoms on this site, in accordance with the following formula [26]:

$$(Mn^{2+}{}_{1-x}\ Ca_x)^{VIII}\ Mn^{3+}{}_6{}^{VI}\ Si^{IV}\ O_{12}\ (\text{with } x \leq 1) \quad (2)$$

where, starting from braunite, within which Mn^{2+} and Mn^{3+}, and not Ca^{2+}, are present, Mn^{2+} is progressively replaced by Ca^{2+}, until the substitution is complete in neltnerite, where Ca^{2+} and Mn^{3+}, and not Mn^{2+}, are identified.

The members of the above series are named as braunite s.s., if $x \leq 0.10$, and calciferous braunite (here defined as Ca-rich braunite) if $0.10 < x < 0.50$; neltnerite is characterised by quite constant stochiometric composition, with x equal to about 1 [26].

In the present study, it was not possible to collect structural data; however, in terms of unit-cell parameters (Figure 4b) the micro-crystals better match with neltnerite rather than braunite [27].

Figure 5 shows a representative situation of a selected inclusion in which the EBSD pattern unquestionably reveals the crystalline nature of all the particles and that each one is composed of one single crystal, randomly oriented in the glass matrix. The comparison of tens of patterns with the internal crystallographic database, unfortunately, did not provide a systematic univocal result, matching with both of the two most probable candidate phases, neltnerite and braunite, due to their very close EBSD diffraction patterns.

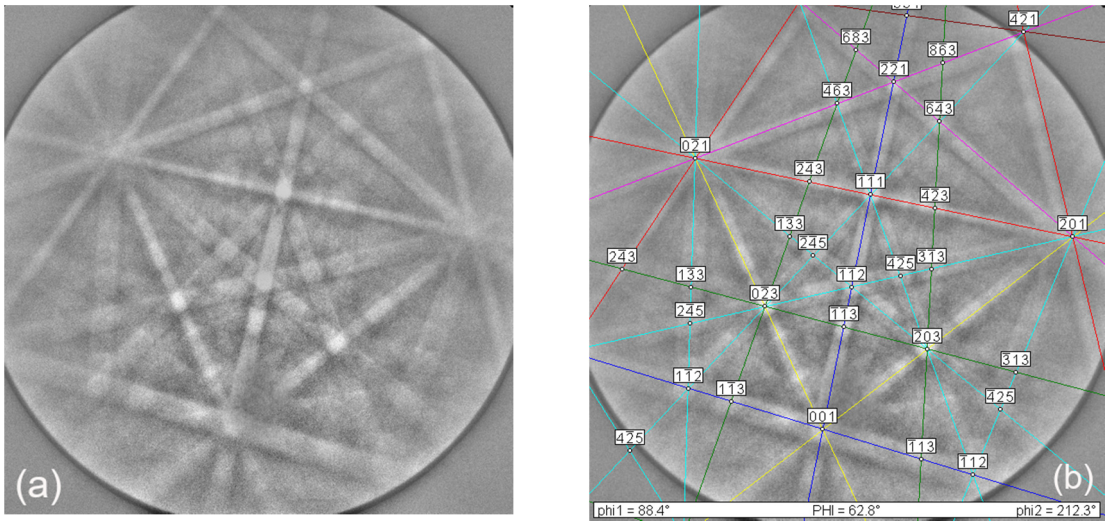

Figure 5. Representative EBSD pattern (**a**) of a manganese-containing inclusion from sample PD-NC1, indexed as neltnerite (**b**).

Micro-Raman spectra carried out on the manganese-containing inclusions (Figure 6) provided further information to distinguish the two phases. The Raman bands are located in the region from 100 to 1000 cm^{-1}, with positions at about 205, 236, 296, 328, 464, 509, 566, 608, 684 and 946 cm^{-1}. The comparisons among the peaks identified in manganese-containing inclusions of Padova tesserae and those identified in the reference spectra of braunite and neltnerite (taking from the RRUFF database) show a better match with the spectrum of braunite, although our spectra are meanly shifted to a lower wavenumber, ca. 10 cm^{-1} for each Raman band and they do not show the band at 986 cm^{-1} (Figure 6), which is also absent in other braunite Raman spectra of the RRUFF database. A comparable shift is also observed in braunite crystals identified in ancient glazed pottery [34,35], and this could be due to cation substitution in the structure of braunite, where Mn^{3+} can be substituted by Fe^{3+} and Al and Mn^{2+} by Ca and little Mg, Cu, Ti, Ba, Na and K [29,31].

These supposed substitutions in the manganese-containing inclusions from Padova tesserae were confirmed by quantitative chemical analyses, carried out by means of EMPA. In particular, inclusions from samples PD-NC1 and PD-PR3, which should be considered representative of all the crystals here identified and analysed in light brown/amber and purple tesserae, respectively, are mainly composed of manganese and silicon (Mn_2O_3 ~88%; SiO_2 ~10%), with small quantities of calcium, magnesium and aluminum, and the absence of iron, titanium and sodium (Table 3).

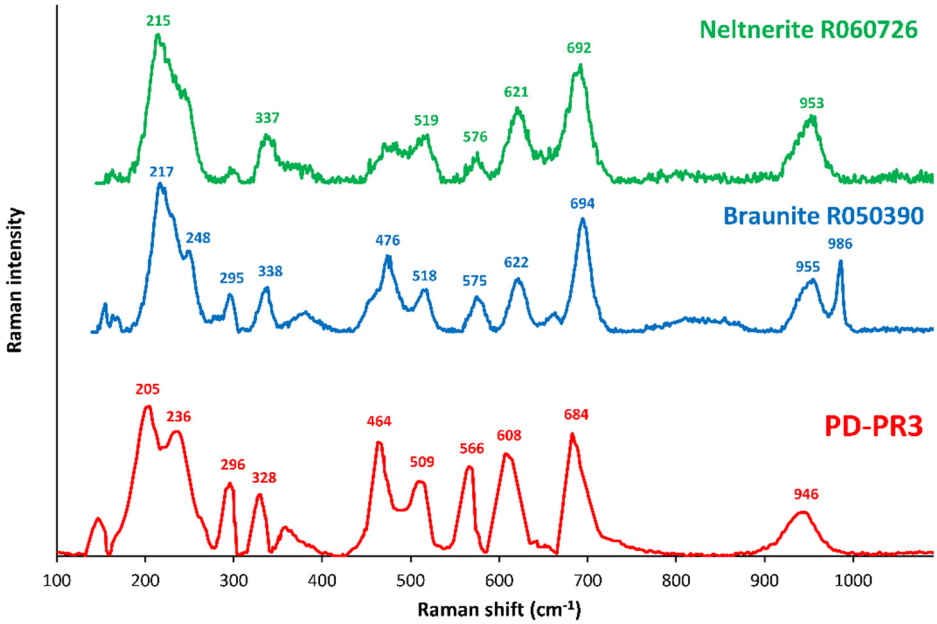

Figure 6. Micro-Raman spectrum, in the region from 100 to 1100 cm^{-1}, of manganese-containing inclusion identified in tessera PD-PR3, compared with the reference Raman spectra of braunite and neltnerite (RRUFF database; RRUFF ID for braunite and neltnerite also shown). Note a better match of PD-PR3 inclusion with the spectrum of braunite R050390, having a chemical formula equal to $(Mn^{2+}_{0.96}$ $Ca_{0.17})$ $Mn^{3+}_{6}SiO_{12}$. Similar micro-Raman spectra are identified in all the other Padova tesserae with manganese-containing inclusions.

Table 3. Mean chemical compositions (in bold) and standard deviations (in italic) of manganese-containing inclusions in tesserae PD-NC1 and PD-PR3, which are representative of all the crystals analysed in Padova tesserae light brown/amber and purple in colours, respectively. Note that chemical compositions of inclusions are quite comparable (EMPA data are expressed as percentual concentrations of element oxides; total manganese and total iron are expressed as Mn_2O_3 and Fe_2O_3, respectively; the number of analyses performed on each sample is about 20).

Sample	Na_2O	MgO	Al_2O_3	SiO_2	CaO	TiO_2	Mn_2O_3	Fe_2O_3	TOTAL
PD-NC1	**<0.02**	**0.35**	**0.11**	**10.01**	**1.82**	**<0.08**	**87.96**	**<0.03**	**100.24**
St. Dev.		*0.08*	*0.06*	*0.21*	*0.07*		*0.36*		
PD-PR3	**<0.02**	**0.27**	**0.19**	**9.82**	**1.88**	**<0.08**	**88.81**	**<0.03**	**100.97**
St. Dev.		0.06	0.03	0.10	0.05		0.30		

Taking into account the EMPA data, the tentative calculation of the stoichiometric formula, on the basis of 12 oxygen ions and about 10% of Mn^{2+}, is reported in the following:

$$\text{PD-NC1: } (Mn^{2+}_{0.740}\ Ca_{0.196}\ Mg_{0.052})^{VIII}\ (Mn^{3+}_{5.987}\ Al_{0.013})^{VI}\ (Si_{1.058})^{IV}\ O_{12} \quad (3)$$

$$\text{PD-PR3: } (Mn^{2+}_{0.743}\ Ca_{0.201}\ Mg_{0.040})^{VIII}\ (Mn^{3+}_{6.013}\ Al_{0.022})^{VI}\ (Si_{0.981})^{IV}\ O_{12} \quad (4)$$

The above formulae are quite comparable, regardless the different colours of tesserae (light brown/amber vs purple), and can be attributed to Ca-rich braunite, having theoretical formula $(Mn^{2+}_{1-x}\ (Ca,Mg)_x)^{VIII}\ (Mn^{3+},\ Al)_6{}^{VI}\ Si^{IV}\ O_{12}$ (with x equal to about 0.25) and "impurities" such as Ca and Mg in distorted cubic coordination, in addition to Mn^{2+}, and Al in the distorted octahedra, in addition to Mn^{3+}, while the Si atoms are only situated into tetrahedrically coordinated position, following the crystal structure of braunite described in de Villiers [23]. These "impurities" may be tentatively attributed to high-temperature interactions with glassy matrices, within which the crystals

are precipitated. At this stage of the study, structural details are still poorly constrained, and future work is needed to better describe the structure of this crystal and the mechanisms of the above atomic substitutions.

Inclusions containing manganese, identified as braunite, have been widely attested in brown and black decorations of ceramic glazes, e.g., in 17th century Portuguese azulejos [34], in Hispano-Moresque glazes from Coimbra [35], in Spanish brown glazes from the 10th to 18th century [36–39], in 17th century tin-glazed ceramics from North-East Hungary [40] and in 19th century polychrome relief tiles from Sintra, and Coimbra in Portugal [41,42], although no specific chemical-crystallographic data on this phase are reported in the cited papers. To the best of the authors' knowledge, this is the first identification of crystals, attributed to Ca-rich braunite, in glass mosaic tesserae.

The occurrence of Ca-rich braunite crystals is particularly important, as it may provide important constrains on melting temperatures of glass tesserae.

Following the same mechanism of natural braunite, which could appear from deoxidation of pyrolusite in the presence of quartz [29], in the case of Spanish brown glaze decoration, Molera et al. [37] supposed that braunite may precipitate from the reaction of pyrolusite, used as source of manganese pigment, with the silica-rich matrix; in the case of 17th century Portuguese azulejos, braunite itself, as local manganese source, is also hypothesised [34]. In addition, according to the MnO-SiO_2 phase diagram, braunite s.s. forms at temperatures of about 500 °C and is stable up to 1150 °C [37,39]. Experiments in the system Mn-Si-O, carried out between 800 and 1100 °C at 1 atm in air, show that, in excess of silica, braunite co-exists with a SiO_2 polymorph (quartz at 800 °C and cristobalite at 1000 °C), and with Mn-pyroxenes at 1100 °C [32,43]. However, it should not be neglected that the incorporation of other elements, like calcium, iron and aluminum in braunite, may have an influence on the phase relations and stability field of crystals at different temperatures, pressures, and oxygen fugacities.

Therefore, in the 14th century Catalan glazes, showing also cassiterite, Molera et al. [37] have hypothesised that braunite is precipitated at temperatures above 1000 °C, by the experimental evidence of coexistence of this phase with Mn-pyroxenes. A similar temperature range was estimated also for 17th century Catalan glazed ceramics, which, having high silicon and low lead and calcium contents in the glazes around the pigment, show only braunite and not Mn-pyroxenes or other Mn-phases, as for the present samples [37].

In the case of late-Antique Padova tesserae, the euhedral habit of crystals indicate that it is a new-formed phase, which had time and space to grow, suggesting that it could be precipitated early during the melting process, from the reaction of pyrolusite, used as source of manganese, with the quartz present in the glass batch. Having in mind both the temperature stability range of braunite s.s. (i.e., 500–1150 °C) and that the studied Ca-rich braunite (and cassiterite, only in light/brown tesserae) is included within a silica-soda-lime glassy matrix, for which a minimum melting temperature of about 950–1000 °C was estimated, it is possible to constrain the melting temperature of tesserae with Mn-containing inclusions between 1000 and 1150 °C. This range is comparable to those of Catalan glazes.

In any case, it is remarkable to note that the same phase is identified in tesserae characterised by different glassy matrices and opacifiers (Table 1). In particular, glassy matrices of NC and PR tesserae are soda-lime-lead and soda-lime in types, and show good chemical comparability with Group 2 and Série 3.2 of Foy et al. [44], respectively. In both chromatic groups, iron and manganese are the colouring elements, with contents comparable for iron (FeO = 0.9 ± 0.2 wt%) and variable for manganese (MnO = 1.3 ± 0.1 and 2.2 ± 0.2 wt% in NC, and PR, respectively). This produces different ratios between these elements, probably explaining different colours of tesserae. In addition, while NC tesserae show cassiterite as opacifier, PR ones have no opacifier [18]. However, the comparability in the micro-textures and in the composition of manganese-containing inclusions, found in all the analysed samples from Padova, suggest that the formation of this phase is not influenced by the chemical compositions of glassy matrix and opacifiers, making its occurrence in glass tesserae as a new potential technological marker.

4. Concluding Remarks

This work reports an unprecedented discovery of manganese-containing inclusions in late-Antique glass mosaic tesserae. The multi-methodological approach applied here has proven to be particularly suitable to clarify the nature of these inclusions, which are also being revealed as new potential technological markers.

The optical, micro-textural and diffraction analyses indicated that the manganese inclusions are a new-formed crystalline phase, which can be mineralogically described as a member of the braunite-neltnerite series.

The micro-textures and chemical composition of this crystalline phase, regardless of the colour, glassy matrices and opacifiers of all the tesserae, suggest a similar production technology, with melting temperatures ranging from 1000 °C to 1150 °C, and pyrolusite as the probable source of manganese in the batch.

Except for some brown and black glazed ceramics, dated to 10th to 19th century AD from Spain, Portugal, and Hungary, within which various manganese bearing crystalline compounds, including braunite, were described, the manganese-containing inclusions identified in this study in the late-Antique tesserae, have never been reported (at least to our knowledge) in any other assemblages of glass mosaic tesserae and vitreous manufacts, in general.

In conclusion, the hypotheses on the production technologies of tesserae with manganese-containing crystalline inclusions, which have been advanced here, still need supplementary experimental verifications (for instance, by means of melting experiments in controlled conditions). Nevertheless, the present study assumes a relevant meaning, because it further demonstrates how the multi-methodological characterisation of inclusions found in glass mosaics allows the current state of knowledge on glass manufacturing in ancient times to be broadened, thereby enlarging the information potentially deductible from samples of different periods and regions.

Author Contributions: Conceptualization and project administration, A.S.; investigation, A.S. (OM, SEM, EMPA, micro-Raman), F.N. (XRD) and L.P. (EBSD).; formal analysis, A.S., F.N. and L.P.; data curation and visualisation, A.S.; funding acquisition, A.S.; writing—original draft preparation, A.S.; writing—review and editing, A.S., F.N. and L.P. All authors have read and agreed to the published version of the manuscript.

Funding: Financial support was provided by the DOR funds of the University of Padova (Project number: DOR1878523/18; principal investigator: Alberta Silvestri).

Acknowledgments: The authors thank the "*Soprintendenza per il patrimonio storico-artistico ed etnoantropologico per le province di Belluno, Padova, Rovigo e Treviso*", and in particular A. Spiazzi, for authorising the archaeometric study, and the Abbot of the Basilica of St. Justine, *Dom.* I. Negrato, for providing Padova tesserae; Serena Tonietto together with P. Guerriero (CNR-ICMATE Padova, Italy), and R. Carampin (CNR-IGG Padova, Italy) for the kind collaboration during SEM-EDS and EMPA analyses, respectively; A. Viani and the Centre of Excellence Telč (Institute of Theoretical and Applied Mechanics of the Czech Academy of Sciences) for the kind support during EBSD analyses; and S. Castelli (Department of Geosciences, University of Padova) for the pictures of the tesserae.

Conflicts of Interest: The authors declare no conflict of interest.

References

1. Biron, I.; Chopinet, M.-H. Colouring, Decolouring and Opacifying of Glass. In *Modern Methods for Analysing Archaeological and Historical Glass*; Janssens, K., Ed.; John Wiley & Sons Inc.: Chichester, West Sussex, UK, 2013; pp. 49–65. ISBN 9780470516140.
2. Bamford, C.R. *Colour Generation and Control in Glass*; Elsevier Scientific Publishing Company: Amsterdam, The Netherlands; Oxford, UK; New York, NY, USA, 1977; Volume 3, ISBN 1520-6378.
3. Schofield, P.F.; Cressey, G.; Wren Howard, W.; Henderson, C.M.B. Origin of color in iron and manganese containing glasses investigated by synchrotron radiation. *Glas. Technol.* **1995**, *36*, 86–94.
4. Freestone, I.C.; Stapleton, C.P. Composition of mosaic glass vessels of the early Imperial period. In *Glass of the Roman World*; Bayley, J., Freestone, I., Jackson, C., Eds.; Oxbow Books: Oxford, UK, 2015; pp. 61–76. ISBN 9781782977742.
5. Newton, R.; Davison, S. *Conservation of Glass*; Butterworth Heineman: Oxford, UK, 1996; ISBN 0750624485.

6. Schreiber, H.D.; Peters, L.J.; Beckman, J.W.; Schreiber, C.W. Redox chemistry of iron-manganese and iron-chromium interactions in soda lime silicate glass melts. *Glas. Sci. Technol.* **1996**, *69*, 269–277.
7. Sayre, E.V. The intentional use of antimony and manganese in ancient glasses. In *Advances in Glass Technology: History Papers and Discussions of the Technical Papers of the VI International Congress on Glass*; Matson, F.R., Rindone, G.E., Eds.; Plenum Press: New York, NY, USA, 1963; pp. 236–282.
8. Jackson, C.M. Making colourless glass in the Roman period. *Archaeometry* **2005**, *47*, 763–780. [CrossRef]
9. Gliozzo, E. The composition of colourless glass: A review. *Archaeol. Anthropol. Sci.* **2017**, *9*, 455–483. [CrossRef]
10. Bidegaray, A.-I.; Godet, S.; Bogaerts, M.; Cosyns, P.; Nys, K.; Terryn, H.; Ceglia, A. To be purple or not to be purple? How different production parameters influence colour and redox in manganese containing glass. *J. Archaeol. Sci. Reports* **2019**, *27*, 101975. [CrossRef]
11. Bidegaray, A.-I.; Nys, K.; Silvestri, A.; Cosyns, P.; Meulebroeck, W.; Terryn, H.; Godet, S.; Ceglia, A. 50 shades of colour: How thickness, iron redox and manganese/antimony contents influence perceived and intrinsic colour in Roman glass. *Archaeol. Anthropol. Sci.* **2020**, *12*, 109. [CrossRef]
12. Silvestri, A. The coloured glass of Iulia Felix. *J. Archaeol. Sci.* **2008**, *35*, 1489–1501. [CrossRef]
13. Peruzzo, L.; Fenzi, F.; Vigato, P.A. Electron Backscatter Diffraction (EBSD): A new technique for the identification of pigments and raw materials in historic glasses and ceramics. *Archaeometry* **2011**, *53*, 178–193. [CrossRef]
14. Schreiber, H.D.; Wilk, N.R.; Schreiber, C.W. Comprehensive electromotive force series of redox couples in soda-lime-silicate glass. *J. Non. Cryst. Solids* **1999**, *253*, 68–75. [CrossRef]
15. Pollard, A.M.; Heron, C. *Archaeological Chemistry*; The Royal Society of Chemistry: London, UK, 2008; ISBN 978-0-85404-262-3.
16. Silvestri, A.; Tonietto, S.; Molin, G. The palaeo-Christian glass mosaic of St. Prosdocimus (Padova, Italy): Archaeometric characterisation of 'gold' tesserae. *J. Archaeol. Sci.* **2011**, *38*, 3402–3414. [CrossRef]
17. Silvestri, A.; Tonietto, S.; Molin, G.; Guerriero, P. The palaeo-Christian glass mosaic of St. Prosdocimus (Padova, Italy): Archaeometric characterisation of tesserae with antimony- or phosphorus-based opacifiers. *J. Archaeol. Sci.* **2012**, *39*, 2177–2190. [CrossRef]
18. Silvestri, A.; Tonietto, S.; Molin, G.; Guerriero, P. The palaeo-Christian glass mosaic of St. Prosdocimus (Padova, Italy): Archaeometric characterisation of tesserae with copper- or tin-based opacifiers. *J. Archaeol. Sci.* **2014**, *42*, 51–67. [CrossRef]
19. Savitzky, A.; Golay, M.J.E. Smoothing and differentiation of data by simplified least squares procedures. *Anal. Chem.* **1964**, *36*, 1627–1639. [CrossRef]
20. Lafuente, B.; Downs, R.T.; Yang, H.; Stone, N. The power of databases: The RRUFF project. In *Highlights in Mineralogical Crystallography*; Armbruster, T., Danisi, R.M., Eds.; De Gruyter: Berlin, Germany, 2015; pp. 1–30. ISBN 978-3-11-041704-3.
21. Geller, S. Structure of alpha Mn_2O_3, $(Mn_{0.983}Fe_{0.017})O_3$ and $(Mn_{0.37}Fe_{0.63})O_3$ and relation to magnetic ordering. *Acta Crystallogr. Sect. B* **1971**, *27*, 821–828. [CrossRef]
22. de Villiers, J.P.R.; Herbstein, F.H. Distinction between two Members of the braunite group. *Am. Mineral.* **1967**, *52*, 20–30.
23. de Villiers, J.P.R. The crystal structure of braunite with reference to its solid-solution behavior. *Am. Mineral.* **1975**, *60*, 1098–1104.
24. de Villiers, J.P.R. The crystal structure of braunite II and its relation to bixbyite and braunite. *Am. Mineral.* **1980**, *65*, 756–765.
25. Baudracco-Gritti, C.; Caye, R.; Permingeat, F.; Protas, J. La neltnérite $CaMn_6SiO_{12}$, une nouvelle espèce minérale du groupe de la braunite. *Bull. Minéral.* **1982**, *105*, 161–165. [CrossRef]
26. Baudracco-Gritti, C. Substitution du manganèse bivalent par du calcium dans les minéraux du groupe: Braunite, neltnérite, braunite II. *Bull. Minéral.* **1985**, *108*, 437–445. [CrossRef]
27. de Villiers, J.P.R.; Buseck, P.R. Stacking variations and nonstoichiometry in the bixbyite-braunite polysomatic mineral group. *Am. Mineral.* **1989**, *74*, 1325–1336.
28. de Villiers, J.P.R.; Dobson, S.M.; Buseck, P.R. Refinement of the crystal structure of neltnerite, a member of the bixbyite-braunite group of minerals. *Eur. J. Mineral.* **1991**, *3*, 567–573. [CrossRef]
29. Bhattacharyya, P.K.; Dasgupta, S.; Fukuoka, M.; Roy, S. Geochemistry of braunite and associated phases in metamorphosed non-calcareous manganese ores of India. *Contrib. Mineral. Petrol.* **1984**, *87*, 65–71. [CrossRef]

30. Sen, S.K.; Dasgupta, H.C. Chemical composition of braunite and bixbyite from Kajlidongri and Tirodi, India. *Indian J. Earth Sci.* **1984**, *11*, 1–28.
31. Velilla, N.; Jiménez-Millán, J. Origin and metamorphic evolution of rocks with braunite and pyrophanite from the Iberian Massif (SW Spain). *Mineral. Petrol.* **2003**, *78*, 73–91. [CrossRef]
32. Abs-Wurmbach, I.; Peters, T.; Langer, K.; Schreyer, W. Phase relations in the system Mn-Si-O: An experimental and petrological study. *Neues Jahrb. Mineral. Abh. J. Mineral. Geochem.* **1983**, *146*, 258–279.
33. Anastasiou, P.; Langer, K. Synthesis and physical properties of piemontite $Ca_2Al_{3-p}Mn_p^{3+}(Si_2O_7/SiO_4/O/OH)$. *Contrib. Mineral. Petrol.* **1977**, *60*, 225–245. [CrossRef]
34. Coentro, S.; Mimoso, J.M.; Lima, A.M.; Silva, A.S.; Pais, A.N.; Muralha, V.S.F. Multi-analytical identification of pigments and pigment mixtures used in 17th century Portuguese azulejos. *J. Eur. Ceram. Soc.* **2012**, *32*, 37–48. [CrossRef]
35. Coentro, S.; Trindade, R.A.A.; Mirão, J.; Candeias, A.; Alves, L.C.; Silva, R.M.C.; Muralha, V.S.F. Hispano-Moresque ceramic tiles from the Monastery of Santa Clara-a-Velha (Coimbra, Portugal). *J. Archaeol. Sci.* **2014**, *41*, 21–28. [CrossRef]
36. Pradell, T.; Molera, J.; Salvadó, N.; Labrador, A. Synchrotron radiation micro-XRD in the study of glaze technology. *Appl. Phys. A* **2010**, *99*, 407–417. [CrossRef]
37. Molera, J.; Coll, J.; Labrador, A.; Pradell, T. Manganese brown decorations in 10th to 18th century Spanish tin glazed ceramics. *Appl. Clay Sci.* **2013**, *82*, 86–90. [CrossRef]
38. Pradell, T.; Molina, G.; Molera, J.; Pla, J.; Labrador, A. The use of micro-XRD for the study of glaze color decorations. *Appl. Phys. A* **2013**, *111*, 121–127. [CrossRef]
39. Di Febo, R.; Molera, J.; Pradell, T.; Vallcorba, O.; Melgarejo, J.C.; Capelli, C. Thin-section petrography and SR-μXRD for the identification of micro-crystallites in the brown decorations of ceramic lead glazes. *Eur. J. Mineral.* **2017**, *29*, 861–870. [CrossRef]
40. Bajnóczi, B.; Nagy, G.; Tóth, M.; Ringer, I.; Ridovics, A. Archaeometric characterization of 17th-century tin-glazed Anabaptist (Hutterite) faience artefacts from North-East-Hungary. *J. Archaeol. Sci.* **2014**, *45*, 1–14. [CrossRef]
41. Coutinho, M.L.; Veiga, J.P.; Alves, L.C.; Mirão, J.; Dias, L.; Lima, A.M.; Muralha, V.S.; Macedo, M.F. Characterization of the glaze and in-glaze pigments of the nineteenth-century relief tiles from the Pena National Palace, Sintra, Portugal. *Appl. Phys. A* **2016**, *122*, 696. [CrossRef]
42. Coentro, S.; da Silva, R.C.; Relvas, C.; Ferreira, T.; Mirão, J.; Pleguezuelo, A.; Trindade, R.; Muralha, V.S.F. Mineralogical characterization of Hispano-Moresque glazes: A μ-Raman and Scanning Electron Microscopy with X-Ray Energy Dispersive Spectrometry (SEM-EDS) study. *Microsc. Microanal.* **2018**, *24*, 300–309. [CrossRef]
43. Abs-Wurmbach, I. Miscibility and compatibility of braunite, $Mn^{2+}Mn_6^{3+}O_8/SiO_4$, in the system Mn-Si-O at 1 atm in air. *Contrib. Mineral. Petrol.* **1980**, *71*, 393–399. [CrossRef]
44. Foy, D.; Picon, M.; Vichy, M.; Thirion-Merle, V. Caractérisation des verres de la fin de l'Antiquité en Méditerranée occidentale: L'émergence de nouveaux courants commerciaux. In Proceedings of the Echanges et Commerce du Verre Dans le Monde Antique, Actes du Colloque de l'Association Francaise Pour l'Archéologie du Verre, Aix-en-Provence et Marseille, France, 7–9 June 2001; Foy, D., Nenna, M.-D., Eds.; Editions Monique Mergoil: Montagnac, France, 2003; pp. 41–85.